SUPPLEMENTARY INFORMATION

1. Supplementary Figure(s) and Legend(s)

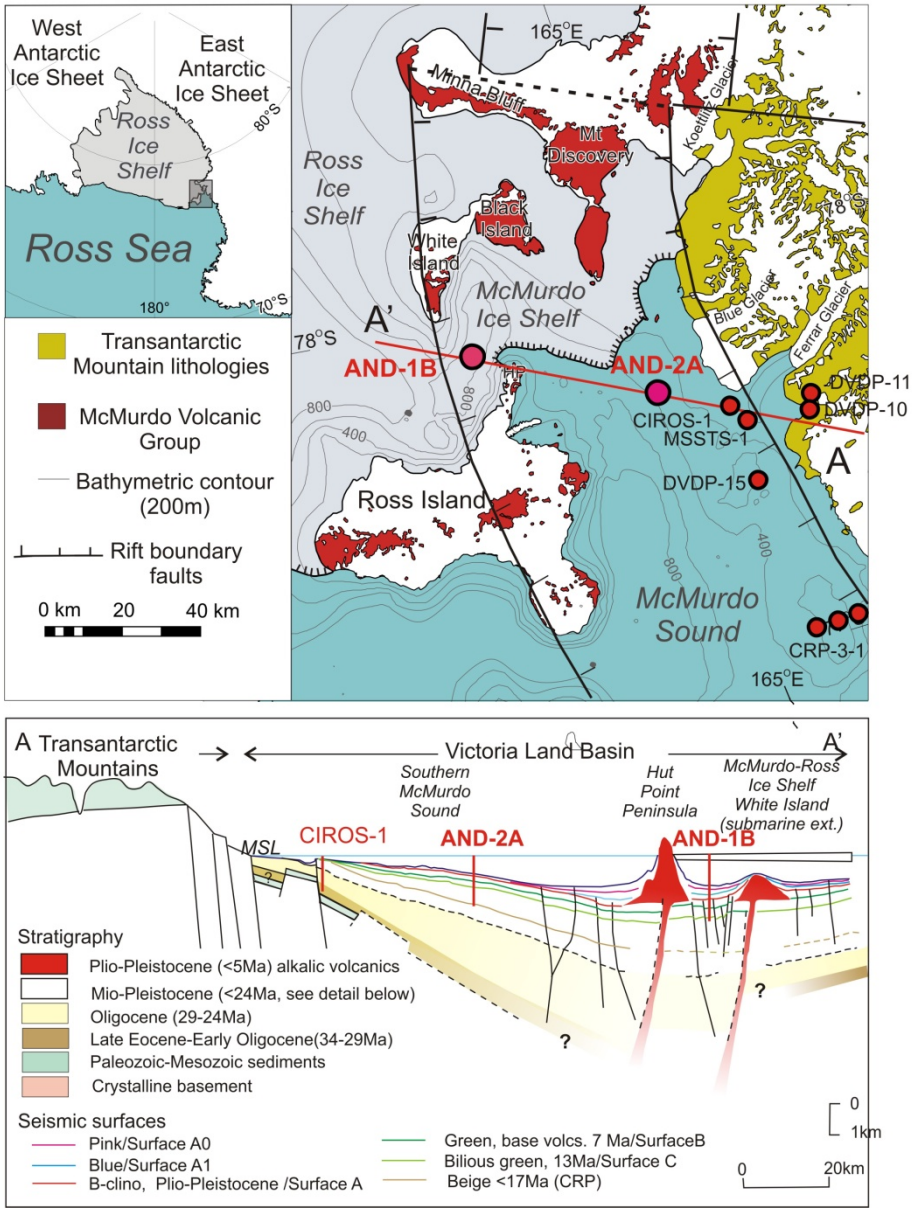

Figure S1. Location of sea-ice and ice-shelf based geological drill core records from the Victoria Land Basin (VLB) in McMurdo Sound. Geological cross-section (A-A') across the VLB shows the stratigraphic relationships and age of strata recovered by the AND-1B core.

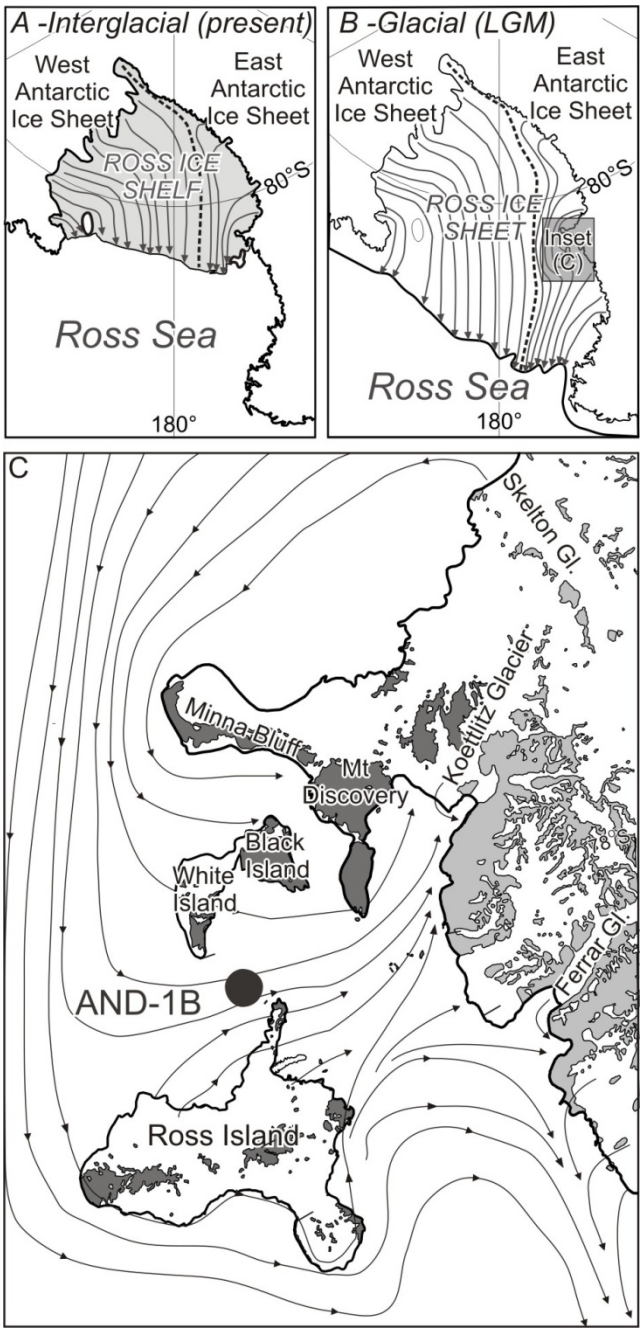

Figure S2. Flow line reconstructions for (A) Holocene[51] and (B) LGM[53] ice sheet/ice shelf configurations in the Ross Embayment, and (C) regional ice flow reconstructed for McMurdo Sound during the LGM[52].

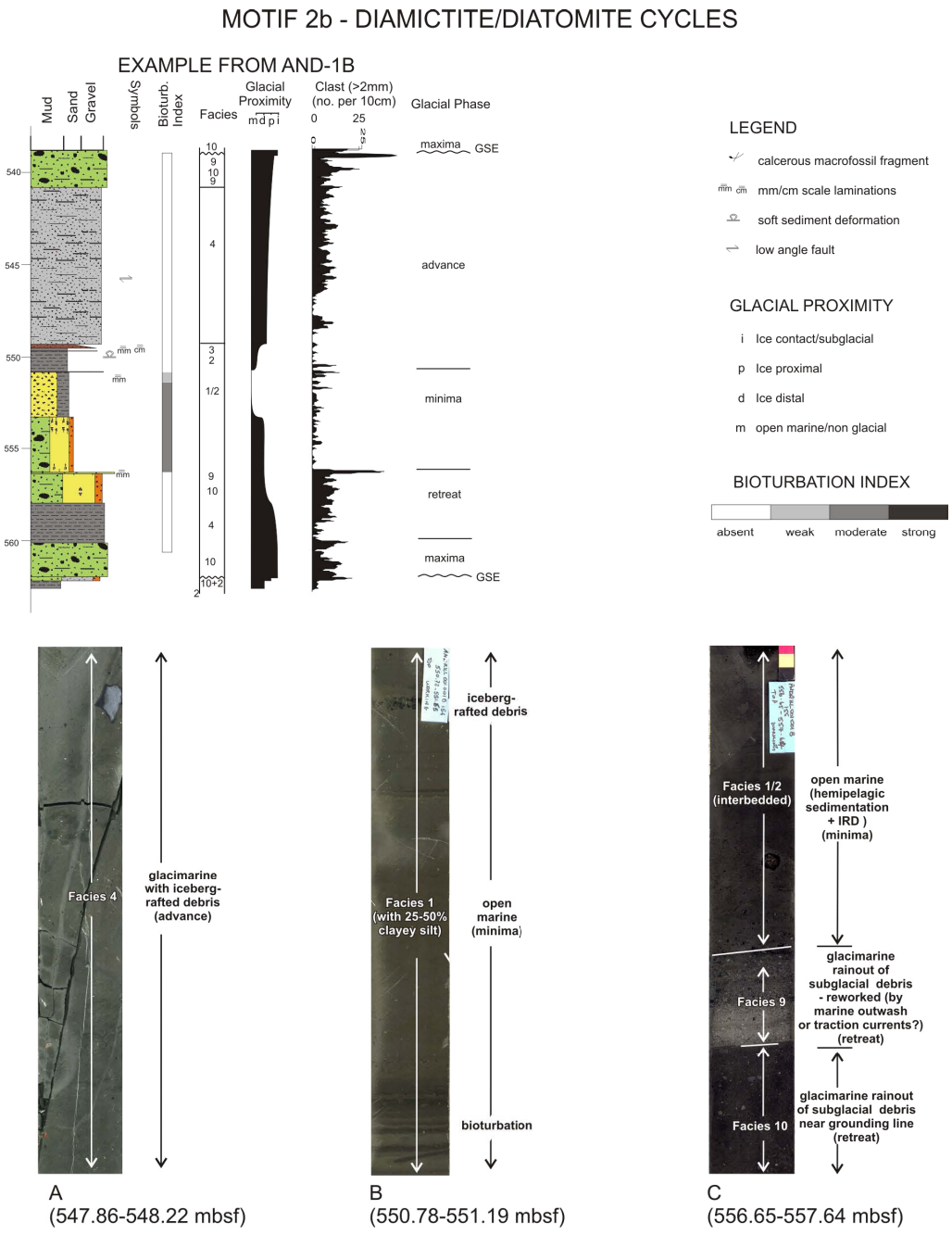

Figure S3 Detailed sedimentological analysis and interpretation of Early Pliocene Cycle 39. An example of a Motif 2B style of subpolar deposition during a 40 kyr cycle of grounding line advance followed by retreat to open ice free oceanic condition and readvance. Facies are summarised in Fig. S2.

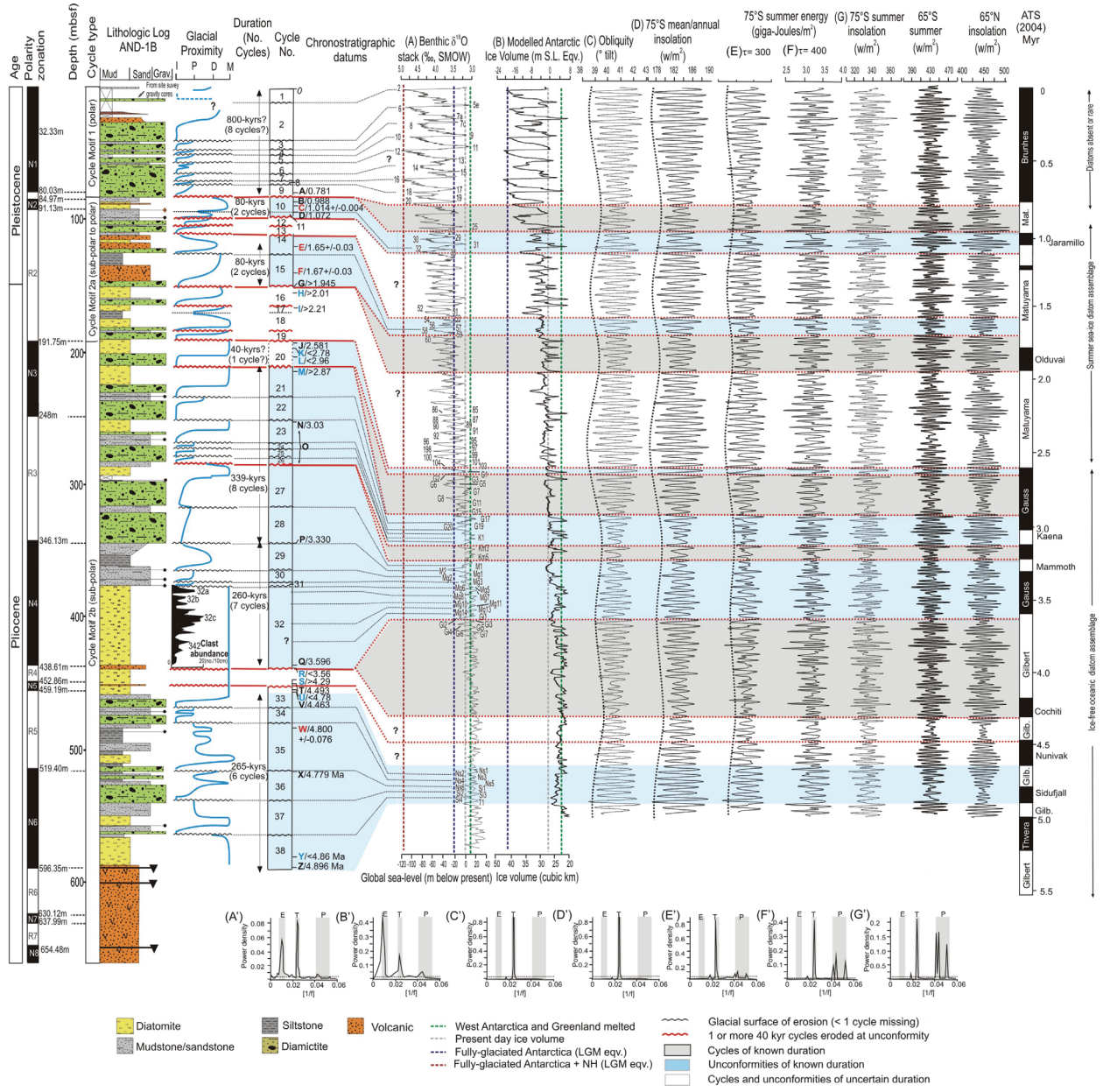

Figure S4. (Expands on Fig. 2) Stratigraphic and chronologic summary of the upper 600m of the AND-1B core showing 40 sedimentary cylces of ice advance-retreat-readvance during the last 5 myrs. Lithologies (rock-types) that comprise the cycles are plotted against depth. Glacial proximity curve tracks the relative position of the grounding line through (i) ice-contact, (p) ice-proximal, (d) ice-distal and (m) marine environments within cycles and provides a proxy for ice extent. Cycle duration is constrained by chronostratigraphic datums coded A-Z and explained in Table S1, and allows correlation of certain intervals of the core with time series of (A) stacked benthic $\delta^{18}O$ record[25], (B) model Antarctic ice volume[7], (C) obliquity, (D) mean annual insolation at 75˚S, (E) summer energy at 75˚S for inferred melt-threshold (τ) of 300 Wm^{-2} and (F) 400 Wm^{-2}, and (G) summer insolation at 75˚S. Summer insolation at 65˚S and 65˚N are also shown.

Spectral estimates show that the majority of the variability is in the obliquity band for (A') $\delta^{18}O$ record, (D') mean annual insolation, and (E') summer energy at 75˚S (τ=300 Wm^{-2}). At a summer melt threshold of τ=400 Wm^{-2}, (F') the variability contains a strong 20,000 year periodicity implying that a colder Pleistocene Antarctic ice sheet system might respond to summer duration at the precessional band[31]. The relative increase in 100 kyr power in (B') model Antarctic ice volume reflects the increased influence of large NH ice sheets and associated glacio-eustatic fluctuations in the Late Pleistocene. E=eccentricity or 100 kyrs, T=tilt or obliquity, P=precession. The notation $\delta^{18}O$ is a measure of the abundance of the ^{18}O isotope relative to mean ocean water (SMOW).

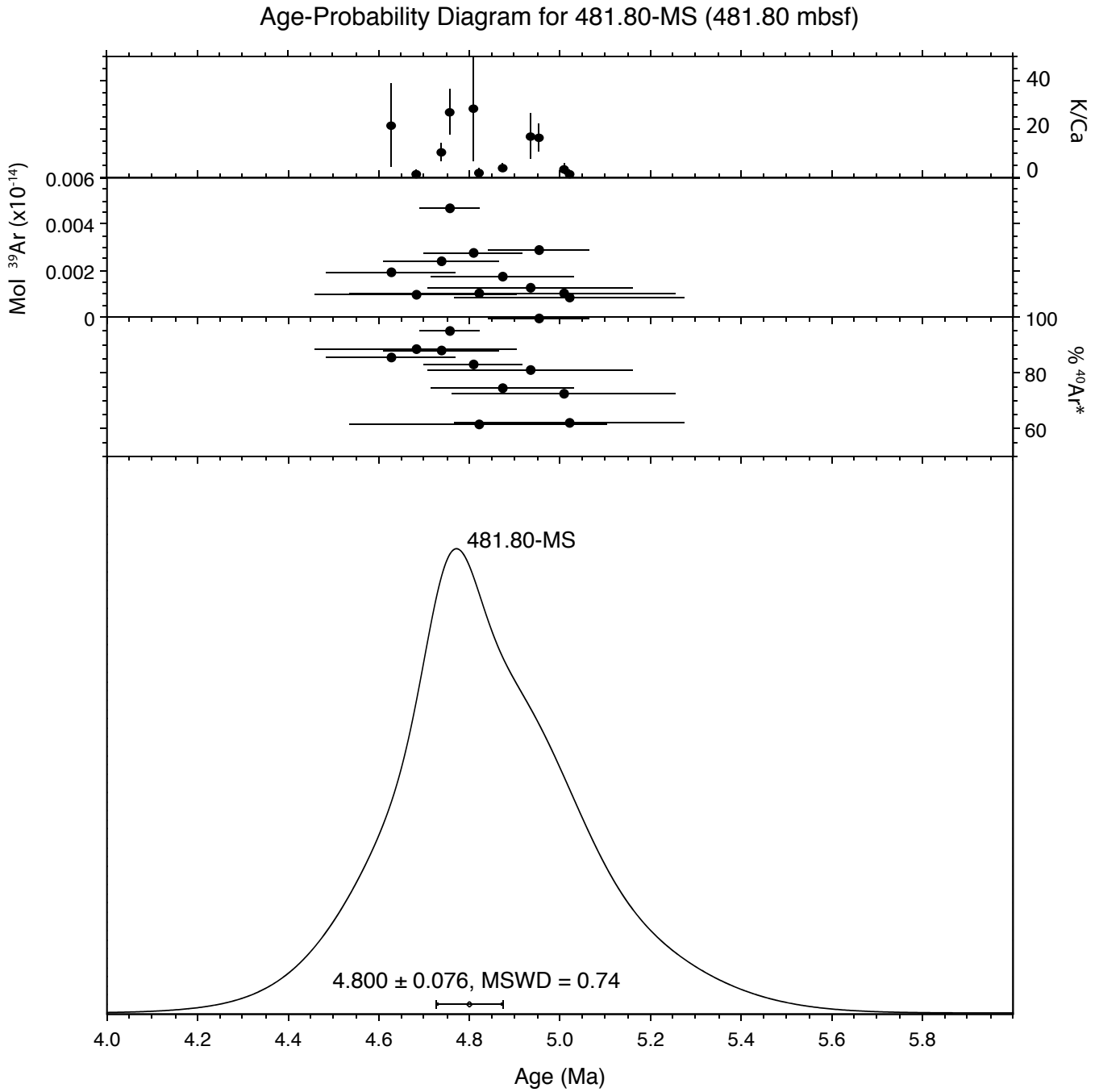

Figure S5. Age-probability diagram for sample 481.80 mbsf showing 11 of the 14 feldspar grains analyzed. Error bars represent 2σ error. Mean standard weighted deviation (MSDW) is also reported to 2σ.

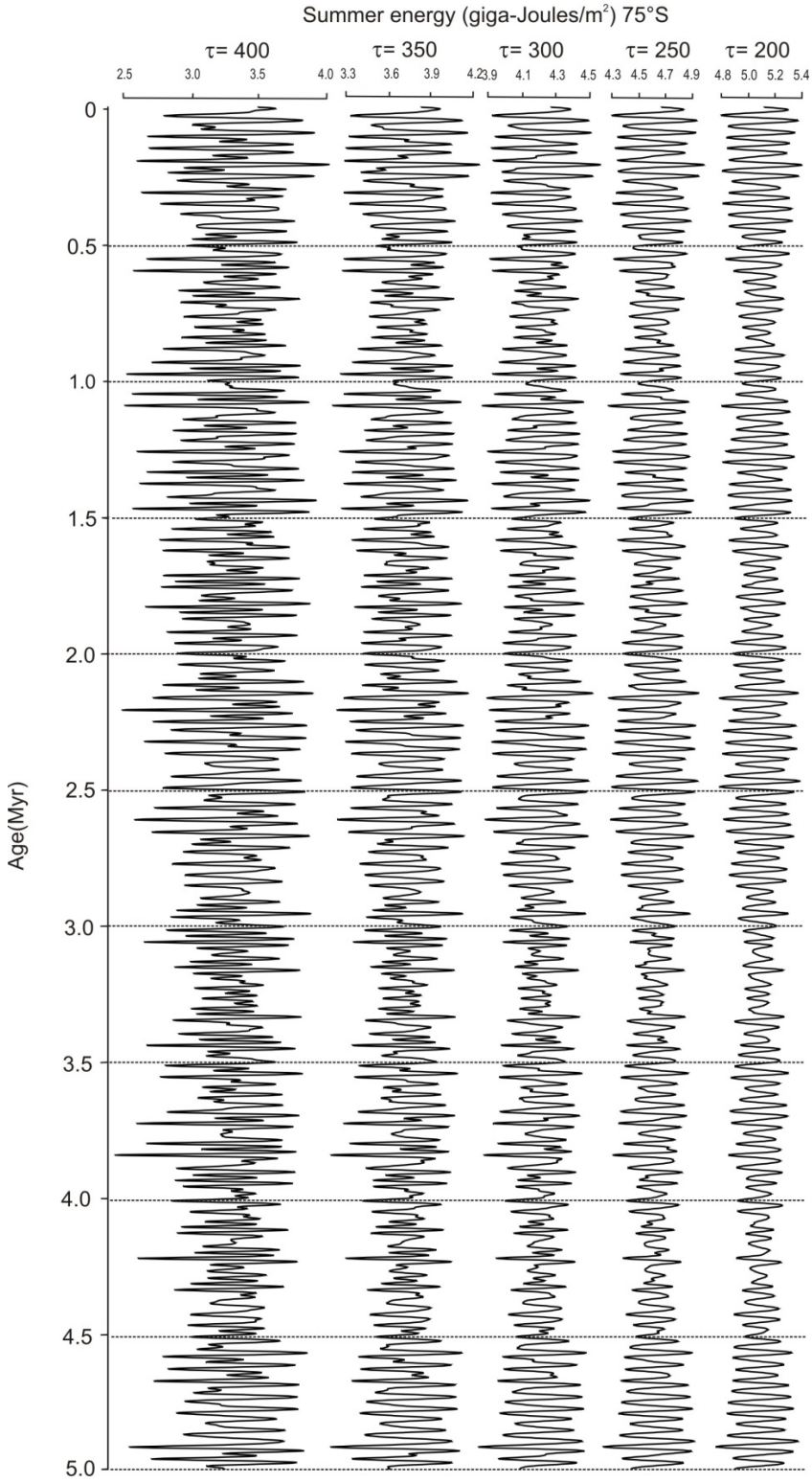

Figure S6. Summer energy at 75°S computed using increasingly higher thresholds (from right to left) following the approach of Huybers[8].

Table S1. Chronostratigraphic constraints for AND-1B

Datum	Depth (mbsf)	Type	Age(Myr)	Error (±)	Comment
A	80.03	paleomagnetic	0.781		Bruhnes-Matuyama transition†
B	84.97	paleomagnetic	0.988		top Jaramillo Subchron†
C	85.50	radiometric	1.014	0.004	$^{40}Ar/^{39}Ar$, K-feldspar‡
D	91.13	paleomagnetic	1.072		base Jaramillo Subchron†
E	112.51	radiometric	1.65	0.03	$^{40}Ar/^{39}Ar$, basaltic glass‡
F	136.21	radiometric	1.67	0.03	$^{40}Ar/^{39}Ar$, basaltic glass‡
G	150.73	paleomagnetic	≥1.945		absence of Olduvai Subchron
H	158.9	biostratigraphic	≥2.01		LO of *Actinocyclus fasciculata*
I	164.1	biostratigraphic	≥2.21		LO of *Actinocyclus maccollumii*
J	191.75	paleomagnetic	2.581		Gauss-Matuyama transition†
K	193.7	biostratigraphic	≤2.79		FO of *A. fasciculata*
L	201.4	biostratigraphic	≤2.87		FO of *A. maccollumii*
M	212		≥2.87		absence of *A. fasciculata* and *A. maccollumii*
N	248.00	paleomagnetic	3.032		Top Kaena Subchron†
O	267.28-282.83	paleomagnetic	3.032 -3.116		4 cycles within Kaena Subchron (112.8-myr-duartion)†
P	346.13	paleomagnetic	3.330		base of Mammoth Subchron†
Q	438.61	paleomagnetic	3.596		Gilbert-Gauss transition†
R	440.12	biostratigraphic	≤3.56		FO of *Rhizosolenia* sp. D *
S	440.12-450	biostratigraphic	≥4.29-4.72		absence of *F.interfrigidaria* and *F. barronii*
T	452.86	paleomagnetic	4.493		Top Nunivak Subchron†
U	456.00	biostratigraphic	≤4.78		FO *of T. striata*
V	459.19	paleomagnetic	4.631		Base Nunivak Subchron†
W	481.80	radiometric	4.800	0.076	$^{40}Ar/^{39}Ar$, K-feldspar‡‡
X	519.40	paleomagnetic	4.799		Top Sidufjall Subchron†
Y	583.64	biostratigraphic	≤4.86		FO of *T. complicata**
Z	596.35	paleomagnetic	4.896		Base Sidufjall Subchron†

*† based on geomagnetic polarity timescale calibration of Ogg & Smith[62], ‡ from Wilson et al.[63], biostratigraphic event ages include the maximum and minimum age identified in the CONOP-constrained Southern Ocean diatom biochronologic calibration of Cody et al.[40], *except which are new (unpublished) ages determined in recent model runs (Cody et al., submitted), ‡‡ see Supplementary Information (below).*

Table S2. Lithofacies, interpretation of depositional process and glacimarine environment for AND-1B

Facies number and name	Predominant process interpretation	Glacimarine depositional environment
1 - Diatomite	Pelagic rain +/- hemipelagic suspension settling (low terrigenous Input)	Open marine Ross Embayment, with or without ice berg rafting
2 - Mudstone	Hemipelagic suspension settling (high terrigenous input)	Open marine Ross Embayment, with or without ice berg rafting
3 - Interstratified mudstone and sandstone	Low to moderate density sediment gravity flow Hemipelagic suspension settling +/-IBRD Redeposition by marine outwash	Distal grounding zone, grounding line fan
4 - Mudstone with dispersed/common clasts	Subglacial deposition Hemipelagic suspension settling Rainout from ice rafting	Proximal to distal grounding zone (polar)
5 - Rhythmically interlaminated mudstone with siltstone or sandstone	Suspension settling from turbid plumes Low-density turbidity current deposition Rainout from ice rafting	Proximal to distal grounding zone (sub-polar)
6 - Sandstone	Sediment gravity flows, fluvial outwash	Proximal grounding zone, grounding line fan
7 - Conglomerate	Redeposition by marine outwash Redeposition by mass flow	Proximal grounding zone, grounding line fan
8 - Breccia	Sediment redeposition by mass flow. Volcanic debris flow.	Proximal grounding zone, grounding line fan
9 - Stratified diamictite	Subglacial deposition Rainout with currents Debris flow depositon	Subglacial to proximal grounding zone
10 - Massive diamictite	Subglacial deposition Rainout without currents Debris flow depositon	Subglacial to proximal grounding zone
11 - Volcanic sediments	Primary volcanics deposits/volcanic debris	Subglacial to open marine

3. Supplementary Discussion

Geological setting of AND-1B drillcore

Ross Island lies at the southern end of the Victoria Land Basin (VLB), an ~ 350-km-long half-graben, hinged on its western side at the Transantarctic Mountain (TAM) front (Fig. S1). Major rifting in the VLB has occurred since the latest Eocene, perhaps having been initiated in the Cretaceous[44,45], and has accommodated up to 10 km of sediment fill. A new rift history, based on the Cape Roberts Project (predecessor to ANDRILL) drill cores linked to a new regional seismic stratigraphic framework[46,47] indicates that crustal stretching during the Oligocene syn-rift phase produced rapid subsidence, followed by thermally-controlled slower subsidence in the Early Miocene. Renewed rifting within the centre of the VLB beginning in the Late Miocene has continued through to present day. This forms the Terror Rift[48], and is associated with alkalic igneous intrusions and extrusive volcanism (e.g. Beaufort Island and Ross Island). Quaternary loading of the crust by the Ross Island volcanoes has added significantly to subsidence near Ross Island, and the development of an enclosing moat[49]. The Terror Rift has accommodated up to 3 km of Neogene sediment beneath Windless Bight. Here, the load-induced subsidence caused by Ross Island has contributed significantly to the generation of accommodation space, especially during the last 2 myr[50]. Neogene strata have now been extensively mapped in southern McMurdo Sound from the Drygalski Ice Tongue south to Ross Island. These Neogene strata show a thickening and eastward-dipping succession extending under Ross Island in the vicinity of the AND-1B drillsite.

Glaciological setting of AND-1B drillcore

AND-1B was drilled at Windless Bight beneath the McMurdo Ice Shelf (Fig. S1) that is an extension of the Ross Ice Shelf at its northwest margin. The McMurdo Ice Shelf has a surface snow accumulation of ~0.3 my^{-1}, and the present day calving line is ~5 km north from the drillsite. Basal melting of the ice shelf is currently occurring at the AND-1B drill site, but the ice is likely free of sediment[27]. The Ross Ice Shelf itself is a major component of the WAIS system with approximately two-thirds of the ice shelf being nourished by ice streams that drain the WAIS, while its western margin is fed by EAIS outlet glaciers[51] (Fig. S2). Reconstructions of grounded ice expansion within the Ross Embayment during the Last Glacial Maximum (LGM)[52] indicate an ice sheet that extended to near the edge of the continental shelf and was fed by a contribution from both East and West Antarctic[53] (Fig. S2).

We have interpreted the glacimarine cycles in AND-1B as documenting retreat and advance of a large marine-based, ice sheet within the Ross Embayment. This ice sheet was/is susceptible to large variations in spatial extent through glacial/interglacial cycles[7]. The provenance of clasts within subglacially deposited diamictites in the AND-1B record are consistent with transport by glacial ice sourced from EAIS outlet glaciers to the south of the drill site[22], indicating that grounded ice events in AND-1B were the result of a large scale advance of the ice sheet across the Ross Embayment, rather than localised glacial advance from Ross Island or outlet glaciers in the McMurdo Sound region.

The ice sheet that occupied the Ross Embayment during past glacial maxima was separated from the high-elevation, land-based sector of the EAIS by the TAM (Fig. S1), and therefore had significantly different mass balance controls and responses to past warm periods. Subglacial sediments in AND-1B were deposited by an ice sheet that was grounded well below sea level. The marine-based ice sheet was highly responsive to oceanic-related mass balance controls, such as eustasy and ocean-induced melting. Model results support this conclusion[7]. Of importance in the model, with regard to ice sheet retreat

within the greater Ross Embayment (including sections of the presently-grounded WAIS), is that marine ice sheet grounding lines are inherently unstable on reverse bed-slopes[e.g.54]. This combined with other forcings such as rising sea-levels, an increased ice sheet temperature profile and/or basal slipperiness is shown to result in rapid, and irreversible retreat. Once retreat was initiated for past configurations of the ice sheet in the Ross Embayment, it was likely to occur across the entire embayment, similar to the pattern of retreat documented for the last deglaciation [e.g52,53,54-56].

Within the McMurdo Sound region, topographic roughness and potential pinning points are provided by the island volcanoes of the Erebus Volcanic Province. Although not fully resolved due to the spatial resolution of the ice sheet model (10 km^2), their influence appears to be relatively minor in comparison to that of ocean warming and eustasy during Pliocene-Pleistocene glacial terminations[7]. Local pinning may delay the eventual collapse/retreat of the ice shelf/ice sheet by a few thousand years during orbital-scale climate cycles. The volcanic edifices of Minna Bluff, Mt Discovery, White Island, Black Island and Ross Island have expressed significant topographic relief above sea level, during the last 5 myr. For example, temporal variations in volcanic activity such as Mt Erebus cone-building[57] are not considered to have fundamentally changed the influence of topographic pinning within the last 1 myr.

Cycle facies motifs and the interpretation of ice sheet thermal regime from AND-1B drillcore

Three distinctive styles of stratigraphic architecture termed “cycle-motifs” have been identified within the entire length of the AND-1B core, and are associated with glacimarine deposition under different thermal regimes of the ice sheet during the last 13.5 myr[22]. Two of the cycle motifs occur in the Pliocene-Pleistocene interval.

1. Polar-type cycles (Motif 1) are dominated by diamictite facies of subglacial and ice-proximal affinity, lack evidence of any significant subglacial meltwater or erosion, and are considered to form under cold, polar conditions with little to no channelised meltwater discharging from the grounding line. This style of depositional cycle provides a stratigraphic signature of advance and retreat of an extensive ice sheet/ice shelf system in the Ross Embayment, similar to Last Glacial Maximum (LGM) to Holocene sedimentary sequences known from the Ross Sea[37] and from beneath the McMurdo Ice Shelf[27].

2. Subpolar-type cycles (Motif 2) contain thick (up to 20 m) intervals of diatomite representing ice free-marine conditions during interglacials. They are divided into two subgroups based on the degree of glacimarine meltwater deposits at the transitions between diamictite and diatomite. Motif 2A cycles (lower meltwater volume) display relatively abrupt transitions between grounding-line proximal deposits and open-marine biogenic sediments as represented by thick deposits of diatomite, with only minor terrigenous content (< 10%). They imply relatively rapid retreat of the WAIS. Thermal conditions of the ice sheet are interpreted as polar to subpolar, warmer than present, yet with limited submarine meltwater and terrigenous sediment supply. Motif 2B cycles typically display a 5- to 10-m-thick terrigenous, glacimarine retreat succession, up to an order of magnitude thicker than in Motif 2A cycles. Similar types of subpolar glacimarine sequences associated with a range of relatively, high meltwater volumes have been described for LGM and Holocene sediments along the marine margin of Greenland[39].

The vertical stacking of cycle motif types is illustrated in Fig. S2 and shows an up-core transition that represents the gradual cooling of the ice sheet, implied by progressively lower volumes of meltwater. Although this is not the primary focus of this paper, evidence for the latter is outlined in a related paper[21]. Here we note on the basis of the characteristics of the grounding-zone facies, and by comparison with modern glacial environments, a reduction of meltwater representing climate cooling and a transition from a subpolar to a polar ice sheet occurs in the AND-1B core ~ 200 mbsf at the level of the Gauss-Matuyama polarity transition (2.6 Myr).

Argon geochronology at 481.80mbsf.

Potassium-feldspar grains from a pumice-rich mudstone interval were separated and analyzed using the $^{40}Ar/^{39}Ar$ method and Single Crystal Laser Fusion technique. The feldspar grains were separated from the pumice-rich layer by crushing and sieving, followed by air abrasion and ultrasonic cleaning to remove any adhering matrix, and lastly handpicked using a binocular microscope to obtain a monomineralic separate. The sample grains were loaded into Al irradiation discs in a known geometry with Fish Canyon Tuff (FC-2) neutron flux monitors (28.02 Myr). The sample irradiation package (NM-214) was irradiated for 1-hour at Texas A&M Nuclear Science Center, College Station, TX. All $^{40}Ar/^{39}Ar$ analyses were conducted at the New Mexico Geochronology Research Laboratory, Socorro, with an automated all-metal UHV extraction line and MAP-215-50 Mass Spectrometer. Samples and flux monitors were fused by a 50 watt Synrad CO_2 laser. Reactive gases were isolated from the sample gas during a 2 minute reaction period with two SAES GP-50 getters, one operated at ~450^{o}C and the other at 20^{o}C. Sample gas was also exposed to a W filament operated at ~2000^{o}C and a cold finger operated at -140^{o}C for addition gas clean-up. Total system blank and backgrounds for laser analyses averaged 56, 1.2, 0.5, 5.3, 0.7 x 10^{-18} moles for masses 40, 39, 38, 37, 36, respectively. Electron multiplier sensitivity averaged 4.95 x 10^{-17} mol/pA for all laser analyses.

When plotted on an age-probability diagram, 11 of the 14 single crystal sanidine and anorthoclase analyses yield a high precision mean age of 4.800 ±0.076 Myr (2σ error) (Fig. S5). The mean age is statistically robust, indicated by a unimodal normal distribution of ages and a mean square weighted deviation close to unity (MSWD =0.74). Analyses 481.80-01-2, 9 and 14 are statistical outliers omitted from mean age calculations. Analysis 481.80-01-2 yields a statistically younger age than the mean. In addition, both the relatively low radiogenic yield (53.4%) and K/Ca (0.79) suggests 481.80-01-2 represents a low potassium or altered grain. Analysis 481.80-01-9 yields an older age than the mean, but a similar radiogenic yield and K/Ca. We infer this analysis to represent an older inherited grain. Analysis 481.80-01-14 has an anomalously low $^{39}Ar_K$ signal (0.006 x10^{-15} mol) and old age (221.6±52.4 Myr, 2σ error). This analysis represents a low potassium, high calcium grain (K/Ca = 2.7) and is likely a xenocryst. The K/Ca values for all analyses used in the mean age calculation exhibit significant variability, ranging from 1.1 to 28.5. This variability in K/Ca, however, does not exceed typical anorthoclase-sanidine ratios and can be accounted for by the analysis of: 1) a zoned feldspar fragmented upon eruption, 2) feldspars from a chemically zoned magma chamber, or 3) material deposited following a vent clearing eruption.

Pliocene summer energy, melt-thresholds and insolation intensity

A further impact of obliquity on high-latitude insolation derives from Kepler's 2nd law, where Earth's distance from the sun is inversely proportional to its angular velocity. Summers with the greatest

insolation intensity, that occur when Earth's orbit is in perihelion at the solstice, are also the shortest due to increased angular velocity, implying that ice sheet ablation may be more sensitive to insolation integrated over the length of the summer (summer energy), than its peak intensity[8]. Fig. S6 shows summer energy at 75°S calculated using different melt-thresholds (τ) following the approach of Huybers[8]. For thresholds of less than 250 Wm^{-2} summer energy varies almost exclusively at the obliquity period. Higher thresholds give greater variability at precession periods as well as greater overall variability. The majority of the variability is at the obliquity period until τ is greater than 340 Wm^{-2}, when precession and obliquity period variance are equal. A warmer-than-present Pliocene climate with minimal sea ice cover in Ross Embayment for the majority of the summer is implied by the diatom assemblage, and suggests an extended period of positive degree-days. For Pliocene southern high-latitudes, the temperature may have been near 0˚C when insolation intensity was around 300 Wm^{-2}. This melt-threshold presently occurs between 40˚-70˚N[8]. Fig. S4 expands upon Fig. 2 and shows correlation of the 40 kyr duration, AND-1B cycles with summer energy curves calculated for τ=300 Wm^{-2} and 400 Wm^{-2} as well as mean annual insolation for the last 5 myr (also shown in detail for chronostratigraphically well-constrained intervals of the core in Figs. 3 & 4).

Summer solstice, insolation intensity for both 65˚N and 65˚S is also plotted in Fig. S4. Seasonal insolation has been proposed to influence Antarctic ice sheet system, both in terms of its intensity[58]and duration[59]. An uncommon orbital configuration produced an extended period of high Antarctic insolation values and warm summers during mid-Pleistocene interglacial MIS 31 (~1 Myr). Geological evidence for ice-free marine conditions in Ross Embayment at this time, together with summer sea-surface temperatures 2-4˚C higher than present was recorded in the sediments of Cape Roberts Project (CRP) cores[33]. The age constraints for the CRP record imply warming driven by southern insolation and Antarctic melt prior to the NH insolation maximum. While we do not dispute the role of seasonal insolation intensity on polar ice volume, especially during times of high eccentricity, our data from the Pliocene AND-1B core (prior to the onset of bipolar glaciations) and the fundamental influence of ocean-induced melting[7] favours the role of mean annual insolation with an additional influence of summer energy, both paced by obliquity, as the first order astronomical control on Antarctic ice volume.

4. Supplementary Notes: Additional References

44. Cooper, A.K. & Davey, F.J. Episodic Rifting of the Phanerozoic rocks of the Victoria Land basin, western Ross Sea. *Antarctica Science,* 229, 1085-1087 (1985).
45. Brancolini, G., et al., Descriptive text for the seismic stratigraphic atlas of the Ross Sea, Antarctica, in *Geology and Seismic Stratigraphy of the Antarctic Margin*, *Antarctic Research. Series, 68,* edited by Cooper, A.K., Barker, P. & Brancolini, G. 271-286, AGU, Washington (1995).
46. Fielding, C.F., Whittaker, J, Henrys, S., Wilson, T & Naish, T.R. Seismic facies and stratigraphy of the Cenozoic succession in McMurdo Sound, Antarctica: implications for tectonic, climatic and glacial history. *Palaeogeography, Palaeoclimatology, Palaeoecology*, 260, 245-261 (2008).
47. Henrys, S.A., Wilson, T.J. Whittaker, J.M., Fielding, C.R., Hall, J.M. & Naish, T.R. Tectonic history of mid-Miocene to present southern Victoria Land Basin, inferred from seismic stratigraphy in McMurdo Sound, Antarctica, in *Antarctica: A Keystone in a Changing World – Online Proceedings of the 10th ISAES*, edited by Cooper, A.K. et al., USGS Open-File Report 2007-1047, Short Research Paper 049 (2007).
48. Cooper, A.K., Davey, F.J. & Behrendt, J.C. Seismic stratigraphy and structure of the Victoria Land Basin, Western Ross Sea, Antarctica, in *The Antarctic Continental Margin: Geology and Geophysics of the Western Ross Sea,* edited by Cooper, A.K. & Davey, F.J. 27-77, Circum-Pacific Council Energy Mineral Resources, Earth Sci. Ser., 5B, Houston, Texas (1987).
49. Stern, T.A., Davey, F.J. &. Delisle, G. Lithospheric flexure induced by the load of the Ross Archipelago, southern Victoria Land, Antarctica, in *Geological Evolution of Antarctica,* edited by Thomson, R.R.A., Crame, A. & Thomson, J.W., Cambridge University Press, Cambridge, UK, 323-328 (1991).
50. Horgan, H., Naish, T., Bannister, S., Balfour, N. & Wilson, G. Seismic stratigraphy of the Ross Island flexural moat under the McMurdo-Ross Ice Shelf, Antarctica, and a prognosis for stratigraphic drilling, *Global Planetary Change,* 45*,* 83-97 (2004).
51. Fahnestock, M.A., Scambos, T.A., Bindschadler, R.A. & Kvaran, G. A millennium of variable ice flow recorded by the Ross Ice Shelf, Antarctica. *Journal of Glaciology*, 46, 652-664 (2000).
52. Denton, G.H. & Hughes, T.J. Reconstructing the Antarctic Ice Sheet at the Last Glacial Maximum. *Quaternary Science Reviews*, 21, 193-202 (2002).
53. Licht, K.J., Dunbar, N.W., Andrews, J.T. & Jennings, A.E. Distinguishing subglacial till and glacial marine diamictons in the western Ross Sea, Antarctica; implications for a last glacial maximum grounding line. *Geological Society of America Bulletin*, 111, 91-103 (1999).
54. Schoof, C. Ice sheet grounding line dynamics: steady states, stability and hysteresis. *Journal of Geophysical Research*, 112, F03S28, doi:10.1029/2006JF000664 (2007).
55. Shipp, S., Anderson, J.B. & Domack, E.W. Late Pleistocene-Holocene retreat of the West Antarctic ice-sheet system in the Ross Sea; Part 1, Geophysical results. *Geological Society of America Bulletin*, 111, 1486-1516 (1999).
56. Conway, H., Hall, B.L., Denton, G.H., Gades, A.M. & Waddington, E.D., Past and future grounding-line retreat of the West Antarctic Ice Sheet. *Science*, 286, 5438, 280-283 (1999).
57. Esser, R.E., Kyle, P.R. & McIntosh, W.C. $^{40}Ar/^{39}Ar$ dating of the eruptive history of Mount Erebus, Antarctica: volcano evolution. *Bulletin of Volcanology*, 66, 671-686 (2004).
58. Kawamura, K. *et al*. Northern Hemisphere forcing of climatic cycles in Antarctica over the past 360,000 years. *Nature* 448, 912–916 (2007).
59. Denton, G. & Huybers, P. Antarctic temperature at orbital timescales controlled by local summer duration. *Nature Geosciences*, doi:10.1038/ngeo311 (2008).
60. Ogg, J.G. & Smith, A.G. The geomagnetic polarity timescale. In *A Geological Time Scale*, Cambridge University Press, Cambridge UK, 63-95, edited by Gradstein et al. (2004).

61. Wilson G., Levy R., Browne G., Dunbar, N., Florindo F., Henrys S., Graham I., McIntosh W., McKay R., Naish T., Ohneiser C., Powell R., Ross J., Sagnotti L., Scherer R., Sjunneskog C., Strong C.P., Taviani M., Winter D. & the ANDRILL-MIS Science Team. Preliminary Integrated chronostratigraphy of the AND-1B Core, ANDRILL McMurdo Ice Shelf Project, Antarctica. *Terra Antartica*, 14, 297-316 (2007).